Composites Part B 84 (2016) 266–276

Contents lists available at ScienceDirect

Composites Part B

journal homepage: www.elsevier.com/locate/compositesb

Progressive failure analysis of three-dimensional woven carbon composites in single-bolt, double-shear bearing

Kyle C. Warren [a, *], Roberto A. Lopez-Anido [a], Senthil S. Vel [b], Harun H. Bayraktar [c]

[a] University of Maine, Advanced Structures and Composites Center, 35 Flagstaff Road, Orono, ME 04469, USA
[b] University of Maine, Mechanical Engineering Department, 5711 Boardman Hall, Orono, ME 04469, USA
[c] Albany Engineered Composites, 112 Airport Drive, Rochester, NH 03867, USA

ARTICLE INFO

Article history:
Received 10 March 2015
Received in revised form
12 August 2015
Accepted 16 August 2015
Available online 8 September 2015

Keywords:
A. 3-Dimensional reinforcement
A. Polymer-matrix composites (PMCs)
C. Damage mechanics
C. Finite element analysis (FEA)
Bolted joints

ABSTRACT

A three-dimensional progressive damage model has been developed to capture the onset and initial propagation of damage within a three-dimensional woven composite in a single-bolt, double-shear joint. Reinforced with a three-dimensional woven ply to ply interlock IM7 carbon fiber preform impregnated with toughened epoxy resin and manufactured using a resin transfer molding process, the composite represents a unique material currently used in select aerospace structures. The modeled joint is commonly found in many aerospace structures and, when combined with the progressive damage response of this three-dimensional woven composite, the material response can be reliably predicted with a three-dimensional non-linear finite element model. This model is constructed using an orthotropic material assumption far from the bearing area and a voxelized mesoscale model with an as-molded geometry representing matrix and impregnated tow phases. The well-established Hashin failure criteria and the Matzenmiller–Lubliner–Taylor damage model were implemented with the unique morphology of three-dimensional woven composites. The onset of damage and trends seen in the model were found to be in agreement with previous experimental findings.

1. Introduction

Three-dimensional (3D) woven composites are used in a variety of aerospace structures. Some of the current applications include fan blades and casings from the CFM International Leading Edge Aviation Propulsion (LEAP) engine, the LiftFan from the Rolls-Royce F-35 Lightning II and landing gear braces from the Boeing 787-8 Dreamliner. Three-dimensional woven composites are attractive alternatives to composites with traditional two-dimensional fiber reinforcement. In addition to improved fracture toughness, notch sensitivity and impact resistance [1,2], three-dimensional woven composites feature near net shape preforming. That is, dry fiber preforms are woven into shapes very similar to the final part geometry. This feature alone has been found to result in reduced material scrap and fabrication labor all at a lower cost [3]. Delamination is effectively eliminated as a potential failure mode because fiber reinforcement is included not only in-plane but also in the through-thickness direction. Three-dimensional woven fiber preforms and composites can be tailored to specific applications. The three-dimensional woven composite discussed in this paper is representative of a typical aerospace composite with three-dimensional fiber reinforcement.

To support expanded use of these unique composites beyond their current applications, an extensive laboratory investigation was conducted to capture the physical material response when subjected to tensile, compressive and shear loading [4]. Efficient bolted joint design requires an in-depth understanding of the bearing behavior of the joined materials. Three-dimensional woven composites have been experimentally evaluated in single-bolt joints in both single-shear and double-shear configurations [5,6]. To enhance this understanding and to support joint design, a numerical prediction tool is needed. This paper describes the development and validation of a progressive damage model for predicting the behavior of composites reinforced with three-dimensional woven ply to ply preforms in single-bolt, double-shear joints. Experimental investigation of three-dimensional woven composites revealed a complex state of bearing damage and failure that included interaction between different tows and matrix material that challenges the classic understanding of bolted

* Corresponding author. Tel.: +1 603 330 2340.
E-mail address: kyle.warren@maine.edu (K.C. Warren).

http://dx.doi.org/10.1016/j.compositesb.2015.08.082

bearing as applied to two-dimensional composites. The modeled joint configuration allows for emphasis to be placed on the material response and development of a progressive damage model for 3D woven composites rather than a particular joint geometry.

Bolted Joints in Composite Aircraft Structures (BOJCAS), a three-year EU-sponsored project that ended in 2003, heavily focused on design of bolted joints on the global and local composite level for use in primary aircraft structures. As part of this effort, finite element models of bolted joints with single and multiple bolts were developed [7–9] and validated experimentally [10–12].

Specifically, McCarthy and McCarthy developed a finite element model to study the effect of bolt hole clearance in single-bolt, single-shear joints [7]. Additionally, the model was extended to multiple fasteners. One of the important conclusions was that as the bolt hole clearance became larger, the joint stiffness was reduced. Results from the study showed good agreement with experimental results.

Perugini, Riccio and Scaramuzzino [8] developed a three-dimensional progressive damage model of a two-dimensional laminated composite using finite element analysis (FEA). Within this paper, a comparison between failure theories and damage models used in the literature found that most of the available models in the research area were derived using two-dimensional FEA. When applied to a single-shear bolted composite configuration, this three-dimensional progressive damage model showed rough correlation with the trends seen in experimental data with clear discrepancies in initial material stiffness. A year later, Riccio and Scaramuzzino [9] improved the earlier model [8] by adjusting the material property degradation rules and, when applied to a different material system, obtained good correlation with experimental results up to about 7% bearing strain.

Ireman [13] has shown that since the through-thickness stress distribution in composite single-shear bolted joints is non-linear, a three-dimensional finite element model should be used to properly capture the through-thickness effects. Included in the BOJCAS project was the continued development of a three-dimensional finite element model by McCarthy and McCarthy [14] of a single-shear, single-bolt joint that was validated with previous experimental work [10] using the same ASTM standard. Part I of this study used a layered model approach with each element representing four plies through the thickness with up to five orthotropic layers per element. The model-predicted joint stiffness was found to be 12.6% higher than the experimental stiffness. The first part of this two-part paper focused on validating the model with experimental results. It should be noted that Part I of this investigation was used exclusively to validate the linear-elastic response of this finite element model when compared with experimental results and does not consider material degradation and failure.

As a continuation of Part I, Part II [15] uses the finite element model developed in Part I to draw comparisons and conclusions from single-bolt, single-shear joints with varied bolt hole clearances. While examining four different levels of clearance, this study concluded that increased bolt-hole clearance results in decreased bolt contact area and a reduction in joint stiffness. Although not used for a progressive damage type analysis, Hashin failure criteria [16] were evaluated near the contact area in the composite to predict the onset of compressive failure in the matrix.

A progressive damage model was presented by Camanho and Matthews [17] for mechanically fastened joints. Their three-dimensional finite element model used Hashin three-dimensional failure criteria [16] coupled with internal state variables that apply degradation factors to material elastic properties for joint failure prediction. In addition to identifying non-critical fiber damage, Camanho and Matthews used a combination of Wang, Hung and Chang's critical damage area as a function of the characteristic distance from the hole [18] and experimental data to determine the final failure prediction to be at the instance in time where accumulated damage has reached the outer edge of the washer. A combination of Tan's work [19], Nuismer and Tan [20,21], and Tan and Perez [22] led Camanho and Matthews to a series of internal state variables that represent material stiffness degradation factors. These factors were determined experimentally for various unidirectional materials for both tensile and compressive failures.

Following the experimental study of a single-bolt, double-shear joint described in Part I [23], Xiao and Ishikawa developed a two-dimensional progressive damage model to predict the joint behavior and reported these results in Part II [24]. The progressive damage model was implemented using a reduction of the compliances via the Abaqus user subroutine USDFLD. Solution dependent variables were used to monitor the values of the failure indicators. When an element in the model was positive for failure based on the failure indicator, a damage variable was then used to modify the material properties.

Zhou et al. [25] investigated the use of a progressive damage model on a plain weave two-dimensional composite unit cell with periodic boundary conditions. Damage initiation in the material was indicated by Hashin failure criteria [16]. The Abaqus user subroutine UMAT was used to modify the stiffnesses of the materials based on prescribed damage variables as a function of the failure criteria. A direct stiffness reduction method was used for elastic property degradation of the epoxy matrix material.

Finite element modeling of mesoscale geometric representations, also called meso-FE, has been described by Lomov et al. in detail in Ref. [26]. Therein, a description of the process for adapting the geometry of a physical composite material into a usable meso-FE model was presented. A description of damage modeling using a mesoscale finite element model was also briefly investigated. Later, Lomov et al. used full-field strain measurement techniques to validate certain aspects of meso-FE modeling. Good correlation was found between the model-predicted surface strains and the measured surface strains [27]. A progressive damage model using a stiffness degradation method was applied to warp-direction loading of a three-dimensional orthogonal woven glass/epoxy composite material and a two-dimensional woven material. Results showed that the simulation predicted the experimentally observed failure modes well [28].

Bogdanovich [1] presented a comprehensive review of the modeling techniques and analysis methods specific to three-dimensional woven composite materials presently and through the recent past. After identifying many challenging research topics in the field of predictive analysis of three-dimensional woven composites, Bogdanovich identified areas that have seen the most attention including elastic property prediction, failure modeling, impact damage modeling, and ballistic impact analysis.

Bogdanovich continued by presenting a progressive failure model of a three-dimensional woven composite unit cell assembled with voxels, or small meso-volumes, using ultimate strain criteria. A damaged state was created by discounting elastic properties of an element once the ultimate strain criteria was satisfied for a particular failure mode. The author cautioned that more complicated failure criteria (including Hashin failure criteria) should be justified and validated with experimental results. Once the failure criteria and method for applying damage is defined, a three-dimensional woven orthogonal geometry was examined. It should be noted that while an orthogonal geometry was considered, the methodology for assigning material properties, orientations, and damage is applicable to any given mesoscale geometric representation. Other research areas discussed were geometry modeling and modeling under complex load cases.

Tsukrov et al. [29] developed a mesoscale finite element model to predict cure-induced microcracking of three-dimensional orthogonal woven and ply to ply woven composites. Representing the as-molded mesoscale geometry with impregnated tow and matrix elements, the model showed good agreement between areas of high parabolic stress within the orthogonal woven material and actual microcracking as observed using micro-CT scans.

Three-dimensional woven modeling strategies were reviewed by Ansar et al. [30]. Included were many approaches to geometry homogenization and averaging techniques as well as applicable failure modes and associated failure criteria. One of the conclusions of the review was that most researchers approached modeling of three-dimensional woven materials with idealized or averaged microstructures. Few were found to incorporate the actual microstructure into the model.

The bulk of the previous work is focused on finite element modeling of bolted connections between composites with two-dimensional fiber reinforcement. Modeling of three-dimensional woven composites is a relatively small research area. This paper introduces a novel research area where a methodical mechanics-based approach is taken to the development of a progressive damage model for composites reinforced with a three-dimensional woven fiber architecture in bolted bearing. A need exists for such progressive damage models to facilitate virtual part prototyping to help extend the current applications for three-dimensional woven composite materials to new components and structures within the aerospace industry.

This paper focuses on a detailed investigation of damage within composite materials with three-dimensional woven fiber reinforcement using a mesoscale finite element model by taking the following research approach:

1. Combine the well-established Hashin failure criteria and the Matzenmiller–Lubliner–Taylor damage model to create a new mechanics-based modeling approach for capturing bearing damage in an as-woven mesoscale geometry representing a three-dimensional woven ply to ply carbon composite.
2. Predict the onset and initial propagation of damage by using a non-linear three-dimensional progressive damage model needed to further joint design and industrial implementation.
3. Validate the progressive damage model by comparing model-predicted failure modes and trends within the bearing stress-strain response with previous experimental findings.

2. Problem description

Damage initiation and propagation is of key interest for understanding the behavior of bolted connections in composites reinforced with three-dimensional woven ply to ply fiber architectures. Experimental methods have been used to determine specific conditions where material degradation is experienced in a single-bolt, double-shear bearing configuration with loading oriented in the warp (longitudinal) tow direction [5]. To supplement laboratory efforts, a finite element modeling approach is taken to develop a progressive damage model to support joint design by predicting the onset and initial propagation of damage. Failure modes and trends in material response evaluated during laboratory characterization are used to validate the numerical methods presented.

The three-dimensional woven ply to ply architecture modeled in this paper is woven with Hexcel 24K IM7 carbon warp and weft tows. The ply to ply angle interlock preform is woven with five tows per weft column and four tows per warp column. The model is representative of an as-molded composite manufactured by Albany Engineered Composites in Rochester, NH using a resin transfer molding process. CYCOM PR-520 toughened epoxy resin is injected into the dry fiber preform to a nominal thickness of 4.19 mm, resulting in a fiber volume fraction of 59.0%. The unit cell size of the molded composite is 10.5 mm in the warp direction and 8.80 mm in the weft direction.

Fig. 1 shows a typical single-bolt, double-shear bearing sample with damage from bearing evaluation. Also depicted is a generic representation of a ply to ply woven fiber architecture, illustrating the orientation of the warp and weft tows within the sample. For additional information about this material system, readers are referred to the experimental work found in Refs. [4] and [5].

3. Characterization of tow and matrix properties

Prior to modeling fiber reinforced composite materials, material properties must be established. Each cluster of fibers, referred to as tows, is impregnated with resin during the molding process. It is important when modeling composite materials with an impregnated tow phase to consider specifically the elastic properties of the impregnated embedded tow. While some manufacturers provide dry fiber properties, impregnated tow properties are dependent upon many factors including the choice of matrix material, tow sizing and the fiber volume fraction within the tows. The fiber volume fraction of impregnated tows is inherently higher than the fiber volume fraction of the composite as a whole. Many numerical and analytical methods exist to predict composite properties of transversely isotropic unidirectional materials. Of particular interest to damage modeling, in addition to elastic tow properties, is the strength of the impregnated tow. Strength and stiffness data obtained from laboratory characterization were used as inputs for the progressive damage model using finite element analysis and is explained in subsequent sections.

To closely resemble the impregnated tows within the three-dimensional ply to ply architecture and mesoscale model, uni-ply panels of IM7 carbon fiber were manufactured by Albany Engineered Composites. Made with a high fiber volume fraction and a low fiber volume fraction, two panels were manufactured with 24K tows and injected with PR-520 toughened epoxy resin using a resin transfer molding process. All carbon fiber reinforcement within the uni-ply panel was oriented in a unidirectional fashion in the longitudinal direction. Tows were woven together with small nylon fibers to maintain fiber alignment during the manufacturing process. While the inclusion of transverse nylon tows precludes this material from being referred to as a true unidirectional, the nylon tows offered very little strength or stiffness as compared with the carbon tows. Minimal carbon tow waviness was noted and is comparable to impregnated tow reinforcement found within the three-dimensional woven ply to ply composite material. Evaluating panels of two different fiber volume fractions allowed for scaling of material properties for various impregnated tow fiber volume fractions without extrapolation. The higher fiber volume fraction panel was found by acid digestion to be 68.3% fiber by volume and the lower fiber volume fraction panel was found to be 61.4%. The voxelized mesoscale model, described in Section 4.1, represents a three-dimensional woven ply to ply fiber architecture. Examination of the number of impregnated tow elements and matrix elements results in the impregnated tow elements containing 69.4% fiber by volume. Tow properties used in the model, as described later in this section, reflect those found experimentally in the high fiber volume fraction material.

Experimental characterization for both impregnated tow materials included tension, compression and in-plane shear and were conducted according to ASTM D3039 [31], ASTM D6641 [32] and ASTM D7078 [33], respectively. All samples were cut on a water jet

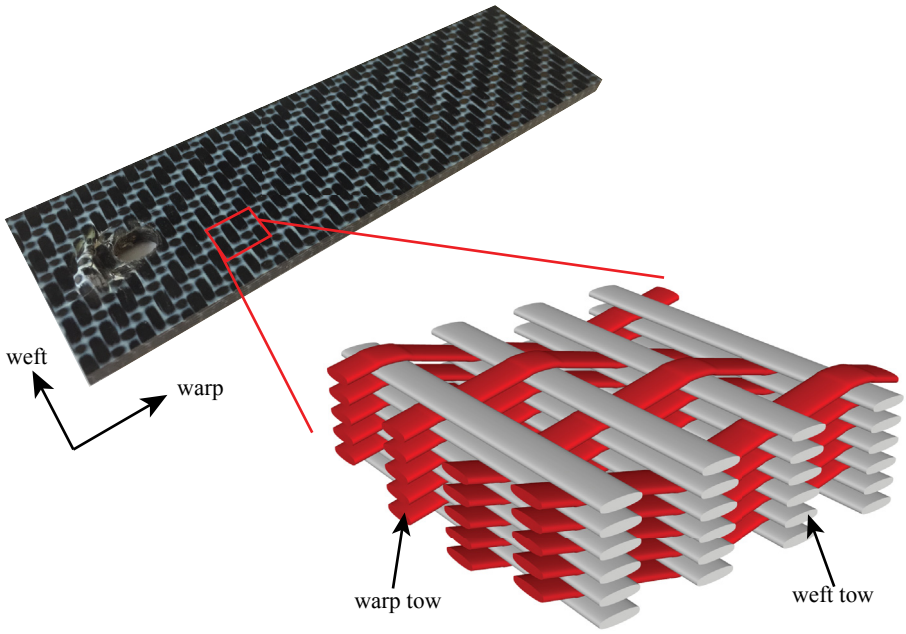

Fig. 1. Single-bolt, double-shear bearing sample with generic ply to ply woven fiber architecture.

and conditioned at 50% relative humidity and a temperature of 23 °C prior to evaluation. Strain was measured during each experiment using ARAMIS, a non-contact digital image correlation (DIC) system.

Both the low and high fiber volume fraction uni-ply materials were evaluated in tensile loading oriented parallel to and perpendicular to the carbon fiber reinforcement. Longitudinal experiments were performed in a 500 kN frame fitted with 250 kN hydraulic grips and a 250 kN load cell. Samples were subjected to a load head displacement rate of 1.27 mm/min. Transverse experimental loading was performed in a 100 kN frame fitted with 100 kN hydraulic wedge grips and a 25 kN load cell. Samples were subjected to a load head displacements rate of 0.508 mm/min. Tensile properties for each of the uni-ply materials are presented in Table 1.

Compression samples were evaluated in a 100 kN frame. A 100 kN load cell was used for longitudinal samples and a 25 kN load cell was used for transverse samples. To ensure the materials experienced quasi-static loading, longitudinal and transverse samples were evaluated at 0.254 mm/min and 0.508 mm/min, respectively. Table 2 lists the compressive modulus and strength for both the low and high fiber volume fraction uni-ply materials.

In-plane shear samples were evaluated with a 25 kN load cell in a 100 kN frame. A displacement rate of 0.635 mm/min was used to evaluate in-plane shear samples under quasi-static loading. Shear strength and modulus for both examined fiber volume fractions are found in Table 3.

Based on this experimental investigation of impregnated tow properties, model inputs were assigned. The elastic material properties and strength properties used in the model to describe the impregnated tow behavior are presented in Table 4 and Table 5,

Table 2
Uni-ply compressive properties.

Material	Compressive strength MPa (COV)		Compressive Modulus GPa (COV)	
	0°	90°	0°	90°
Low v_f –61.4%	665 (5.26%)	177 (2.24%)	144 (3.83%)	8.48 (4.19%)
High v_f –68.3%	673 (8.33%)	172 (3.01%)	168 (6.35%)	9.51 (5.42%)

Table 3
Uni-ply shear properties.

Material	Shear strength MPa (COV)	Shear Modulus GPa (COV)
Low v_f –61.4%	106 (6.16%)	5.30 (11.8%)
High v_f –68.3%	105 (5.14%)	6.67 (5.95%)

Table 4
Impregnated tow elastic material properties.

Elastic properties	
E_1	180 GPa
E_2	9.45 GPa
E_3	9.45 GPa
ν_{12}	0.433
ν_{13}	0.433
ν_{23}	0.465
G_{12}	6.67 GPa
G_{13}	6.67 GPa
G_{23}	3.23 GPa

Table 1
Uni-ply tensile properties.

Material	Tensile strength MPa (COV)		Tensile Modulus GPa (COV)		ν_{12} (COV)
	0°	90°	0°	90°	
Low v_f –61.4%	1750 (2.34%)	69.6 (3.54%)	158 (1.35%)	8.48 (1.51%)	0.414 (3.07%)
High v_f –68.3%	1860 (2.69%)	58.6 (2.79%)	180 (1.43%)	9.45 (1.94%)	0.433 (3.81%)

Table 5
Impregnated tow strength properties.

Strength Parameter (direction)	Symbol	Strength (MPa)
Longitudinal Tensile (1)	S_1^T	1810
Longitudinal Compressive (1)	S_1^C	669
Transverse Tensile (2, 3)	$S_2^T = S_3^T$	64.0
Transverse Compressive (2, 3)	$S_2^C = S_3^C$	174
Shear (1–2,1–3)	$S_{12}^F = S_{13}^F$	105
Shear (2–3)	S_{23}^F	105

Table 6
Isotropic epoxy matrix properties (PR-520)[34].

Property	Symbol	Value
Elastic Modulus (GPa)	E	4.00
Poisson's Ratio	ν	0.398
Tensile Strength (MPa)	Y_T	82.1
Compressive Strength (MPa)	Y_C	128
Shear Strength (MPa)	τ_{ult}	61.4

respectively. Fig. 2 defines the reference material orientation for transverse isotropy for impregnated tows. The out of plane shear modulus and Poisson's ratio were not determined experimentally. A typical value of ν_{23} was assumed and the shear modulus was calculated using ν_{23} and E_2 with isotropic assumptions. Similarly, the shear strength in the 2–3 plane was assumed to be the same as the shear strength calculated in the 1–2 plane due to the difficulty of evaluating this shear property experimentally. Table 6 contains the elastic and strength properties for the matrix material that were used as model inputs [34].

4. Finite element model

Similar to a specimen described in ASTM D5961 Procedure A [35], a simple geometry was considered for the progressive damage model. Controlled by a linearly ramped displacement of 0.794 mm (corresponding to approximately 12% bearing strain), a 6.35 mm steel pin was used to impart bearing stress on the composite material. As described in a later section, the model was terminated before completing this displacement. Bearing strain is the amount of hole deformation in the direction of loading divided by the hole diameter. According to the Standard, bearing strain is measured between the fixture and the composite sample. Bearing strain was measured in the model to replicate as closely as possible the measurement of experimental bearing strain by recording the relative displacement of a node on the pin to a node far from the hole on the composite. The distance between these nodes corresponded closely to what a mechanical extensometer with a 50.8 mm gage length would capture. Gripping of the sample was considered in the model as a fixed boundary condition. Penalty contact was included between the steel pin and the composite material along the bearing surface with a coefficient of friction of 0.1. Model dimensions and loading conditions are illustrated in Fig. 3.

4.1. Mesoscale model

A representative volume element (RVE) of fiber reinforced composite material can be defined as the smallest collection of microstructure or microstructure constituents that accurately represent the behavior of the macrostructure of the composite. For a composite material, an RVE typically includes both the fiber reinforcement as well as the matrix material. In the case of three-dimensional fiber reinforcement, an RVE is used that represents a repeating pattern in the weave architecture and contains both matrix and fiber tows. This level of constituent material representation is referred to as a mesoscale [27]. A voxelized mesoscale model representing as-molded impregnated tow and matrix geometries was used as the basis for more complex models. A similar geometric representation is described in detail in Ref. [36]. A representation of the mesoscale model is illustrated in Fig. 4.

The mesoscale model was considered with two different mesh densities. The coarsely meshed model (1.27 million degrees of

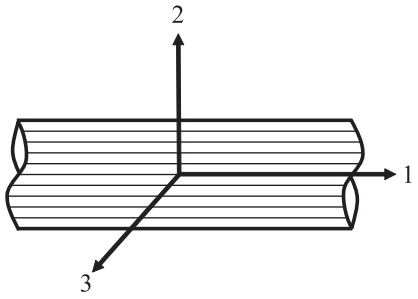

Fig. 2. Impregnated tow material orientations.

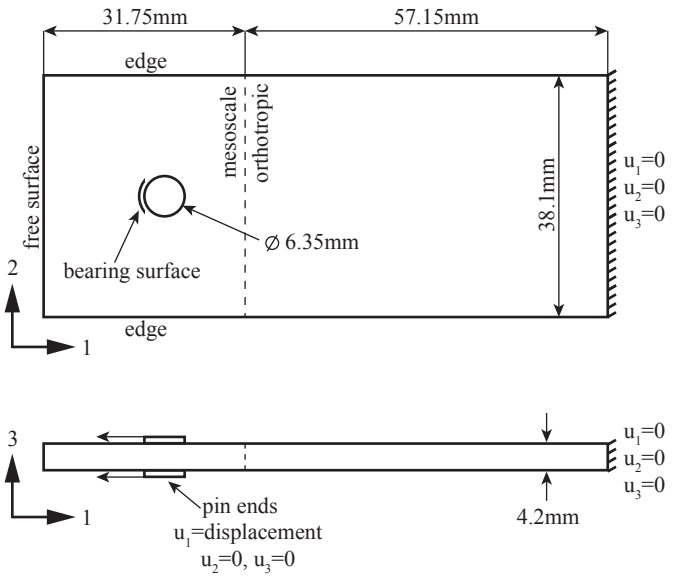

Fig. 3. Model geometry and loading conditions.

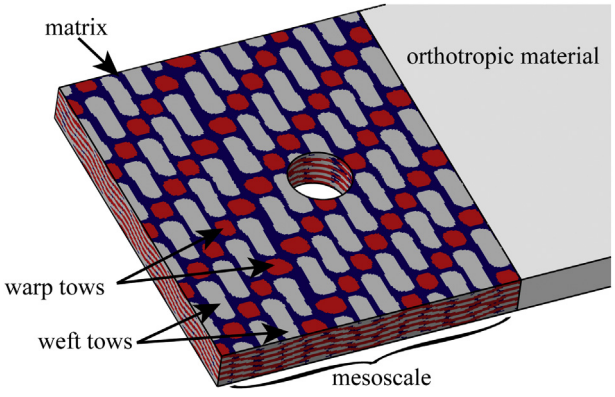

Fig. 4. Mesoscale model representation.

freedom) was used to evaluate modeling parameters for run-time efficiency. The finely meshed model (7.86 million degrees of freedom) was assumed to be geometrically converged and was used for all presented comparisons. The voxelized mesoscale geometry and pin utilize C3D8 elements within Abaqus, representing 8-noded, fully integrated solid continuum brick elements. The orthotropic composite material was modeled with C3D8R, 8-noded continuum brick elements with reduced integration.

4.2. Progressive damage model

A suitable failure criterion is required to capture the progressive damage of composite materials using finite element analysis. Failure criteria are expressions or sets of expressions that, when evaluated, predict failure in one or more specific failure modes. Many different failure criteria exist for a variety of materials and applications. For unidirectional fiber-reinforced composites, failure criteria developed by Hashin [16] are commonly used. Three-dimensional Hashin failure criteria assess the integrity of transversely isotropic impregnated material in four modes: fiber tensile, fiber compressive, matrix tensile, and matrix compressive. A means of applying damage or a degraded response to the material is also required. The method utilized in this progressive damage model is commonly applied to composite materials and was initially developed by Matzenmiller, Lubliner and Taylor [37].

In addition to failure criteria that predict modes in which material failure can occur and a damage model that can apply failure criteria to effect physical changes in the material, a means of applying material change in a finite element analysis must be used. The MLT damage model is not specific as to effecting damage to the compliance matrix or to the stiffness matrix and an option exists for both using Abaqus. For implicit modeling, Abaqus user subroutine USDFLD is commonly used to apply damage to parts of the compliance matrix by directly degrading elastic material properties. Progressive damage in this three-dimensional woven composite material was modeled in this manner by modifying the engineering constants of the damaged materials.

The experimental bearing response of three-dimensional woven materials is unique. After damage onset, propagation of damage occurs without a significant loss in load-carrying capacity. In other words, as bearing strains increase after initial bearing failure, the bearing stress remains relatively constant, resulting in a zero-stiffness response. In implicit finite element modeling, capturing a material response with zero stiffness is not practical. The use of explicit modeling and element deletion, signifying complete property degradation and failure, should be used to predict the material response at high bearing strains. Capturing the onset and initial propagation of damage in this three-dimensional woven composite is more important for joint design than capturing the entire bearing response with significant bearing failures. The progressive damage model presented describes the material response as it begins the transition from a linear-elastic behavior to a non-linear damaged state. For this reason, implicit modeling was most appropriate and the progressive damage model was terminated when significant bearing failure was detected.

User-defined field variables were used to degrade select elastic material properties. A damaged compliance matrix was calculated at each material point by considering the stress state at each point during the previous increment. When using implicit modeling, convergence is not dependent upon the time step between increments since equilibrium conditions are enforced during each increment. Since the material properties in the current increment are a function of the stress state in the previous increment, it is important to control the time stepping and to keep the step sufficiently small to allow a converged damaged material solution.

The mesoscale finite element model incorporated two different material phases: warp and weft impregnated tows and matrix material. Each individual element of the impregnated tow was modeled as transversely isotropic material with material orientations prescribed in such a way that described the physical geometry of a three-dimensional ply to ply woven material. Each matrix element was modeled as an isotropic material. The following sections describe the application of Hashin failure criteria, damage variables and damage evolution to the finite element model.

4.2.1. Hashin failure criteria and failure indicators

Hashin failure criteria were adopted for impregnated tow elements. Using this model, both longitudinal and transverse tension and compression were acceptable tow failure modes. Additionally, combination failure modes that include shear damage were considered. Hashin failure criteria [16] are presented in Table 7 and have been found by others to work well in bolted configurations [17,38–40]. Failure indicators f_1, f_2, f_3 and f_4 represent each of the four failure modes considered in the impregnated tow material damage model. The value of each failure indicator was determined by using $F(\boldsymbol{\sigma}/f) = 1$ by solving the equation for each failure mode for f where $\boldsymbol{\sigma}$ is the stress tensor. Failure occurred in a particular mode when the corresponding failure indicator reached a value greater than or equal to 1.

For the two matrix mode failure indicators (f_3 and f_4), σ_{22} and σ_{33} are the principal stresses within the 2–3 plane. All of the other stress values correspond to the material orientations as defined in Fig. 2. Strength values referred to in the Hashin failure criteria in Table 7 are given in Table 5.

4.2.2. Damage variables

Failure indicators were used to calculate damage variables (DVs) which affect the material behavior. In this progressive damage model, damage variables directly affected the elastic properties of a material by modifying the diagonal components of the compliance matrix at each material point on an element-by-element basis. The derivative of each damage variable d with respect to each failure indicator f was always greater than or equal to zero. That is, once damage occurred, material 'healing' was prevented. Four damage variables were used, with prescribed values in the interval [0,1]. The four damage variables, all functions of the specific failure indicators as seen in Table 8, were used to modify the material compliance matrix. The damaged compliance matrix as a function of the damage variables is shown in Equation (1). Off-diagonal terms within the compliance matrix remain unaffected by damage variables in order to satisfy physical and thermodynamic conditions. The derivation of this damaged compliance matrix is described in detail by the MLT model [37].

$$S(d) = \begin{bmatrix} \frac{S_{11}}{1-d_1} & S_{12} & S_{13} & 0 & 0 & 0 \\ S_{12} & \frac{S_{22}}{1-d_2} & S_{23} & 0 & 0 & 0 \\ S_{13} & S_{23} & \frac{S_{33}}{1-d_2} & 0 & 0 & 0 \\ 0 & 0 & 0 & \frac{S_{44}}{1-d_3} & 0 & 0 \\ 0 & 0 & 0 & 0 & \frac{S_{55}}{1-d_3} & 0 \\ 0 & 0 & 0 & 0 & 0 & \frac{S_{66}}{1-d_4} \end{bmatrix} \quad (1)$$

Table 7
Hashin failure criteria.

Failure Mode and condition	Failure criteria
Tensile fiber $\sigma_{11} > 0$	$F_1(\boldsymbol{\sigma}) = \left(\frac{\sigma_{11}}{S_1^t}\right)^2 + \frac{1}{(S_{12})^2}(\sigma_{12}^2 + \sigma_{13}^2) = 1$
Compressive fiber $\sigma_{11} < 0$	$F_2(\boldsymbol{\sigma}) = \frac{-\sigma_{11}}{S_1^c} = 1$
Tensile matrix $\sigma_{22} + \sigma_{33} > 0$	$F_3(\boldsymbol{\sigma}) = \frac{1}{(S_2^t)^2}(\sigma_{22} + \sigma_{33})^2 + \frac{1}{(S_{23}^t)^2}(\sigma_{23}^2 - \sigma_{22}\sigma_{33}) + \frac{1}{(S_{12}^t)^2}(\sigma_{12}^2 + \sigma_{13}^2) = 1$
Compressive matrix $\sigma_{22} + \sigma_{33} < 0$	$F_4(\boldsymbol{\sigma}) = \frac{1}{S_2^c}\left[\left(\frac{S_2^c}{2S_{23}^t}\right)^2 - 1\right](\sigma_{22} + \sigma_{33}) + \frac{1}{4(S_{23}^t)^2}(\sigma_{22} + \sigma_{33})^2 + \frac{1}{(S_{23}^t)^2}(\sigma_{23}^2 - \sigma_{22}\sigma_{33}) + \frac{1}{(S_{12}^t)^2}(\sigma_{12}^2 + \sigma_{13}^2) = 1$

Damage variables seen in Equation (1) were implemented in Abaqus using the USDFLD Fortran user subroutine. DVs were stored as field variables (FVs) in Abaqus and were implemented by using a table of material property dependencies. Failure indicators were stored as Solution Dependent Variables (SDVs) and can be monitored throughout the progression of the model.

4.2.3. Damage evolution

Damage evolution refers to how the value of the damage variable is prescribed. The longitudinal and transverse damage variables d_1 and d_2 are related to the Hashin failure indicators through the damage evolution function α as listed in Table 8. Damage variables d_3 and d_4, representing shear damage, were considered to be a combination of longitudinal and transverse damage, and were therefore assumed to be dependent upon d_1 and d_2. The damage evolution function $\alpha = \alpha(f)$, as seen in the damage variable definitions in Table 8, can be used to enforce various damage evolution laws including instantaneous damage (brittle failure) or a nonlinear relationship, representing a more ductile failure, as a function of the failure indicators. Equation (2) describes the instantaneous damage evolution law as it was applied to the matrix material.

$$\alpha(f) = \begin{cases} 0, & \text{if} \quad f < 1 \\ d_{max}, & \text{otherwise} \end{cases} \tag{2}$$

The value of the damage evolution function $\alpha(f)$ is either 0, representing undamaged, or d_{max}, representing a complete material failure. d_{max}, when applied using the MLT model with instantaneous damage, represents the percentage of elastic property degradation from the original. McCarthy [40] investigated multi-fastener damage in a 2D composite (HTA/6376), and used a maximum damage of $d_{max} = 0.90$, corresponding to degraded (damaged) elastic properties to 10% of their original values. In this progressive damage model, the instantaneous damage evolution law from Equation (2) was applied in combination with a maximum principal stress failure criterion to capture damage in the matrix material phase using $d_{max} = 0.90$.

Following an exponential damage law, seen in Equation (3), damage was applied to impregnated tow elements. This damage evolution model incorporated a material response parameter m. As this parameter increased, the more brittle-like the material damage response becomes. This parameter must be tuned for the impregnated tow material phase. As the parameter approaches an infinite value, the exponential damage evolution model becomes an instantaneous damage model. Refer to Table 8 for definitions of each damage variable d for impregnated tow elements. Each damage variable d was calculated from the exponential damage evolution law $\alpha = \alpha(f)$ seen in Equation (3) where e is the base of the natural logarithm. To better illustrate the relationship between the failure indicator f and the damage variable d through the exponential damage evolution function $\alpha(f)$, a plot of Equation (3) is shown in Fig. 5 with $d_{max} = 0.80$ evaluated at various values of the material response parameter m.

Table 8
Damage variable definitions.

Damage mode	Damage variable value
Longitudinal damage (fiber)	$d_1 = \alpha(\max\{f_1, f_2\})$
Transverse damage (matrix)	$d_2 = \alpha(\max\{f_3, f_4\})$
Longitudinal shear (combined)	$d_3 = 1-(1-d_1)(1-d_2)$
Transverse shear (combined)	$d_4 = d_3$

$$\alpha(f) = d_{i\,max}\left[1 - \exp\left(-\frac{f^m}{m\,e}\right)\right] \tag{3}$$

The final component of the progressive damage model is the specification of d_{max} for various impregnated tow element failure modes. In other words, the residual engineering stiffnesses for impregnated tow elements must be specified for each of the considered failure modes. Based on previous work by Tan and Perez [19,22] and Camanho and Matthews [17], material degradation factors for tow damage were applied to the progressive damage model. Considered independently for tensile and compressive damage in both the longitudinal and transverse directions, these maximum degradations are seen in Equations (4) and (5).

$$d_{1max} = \begin{cases} 0.93, & \text{if tension} \\ 0.80, & \text{if compression} \end{cases} \tag{4}$$

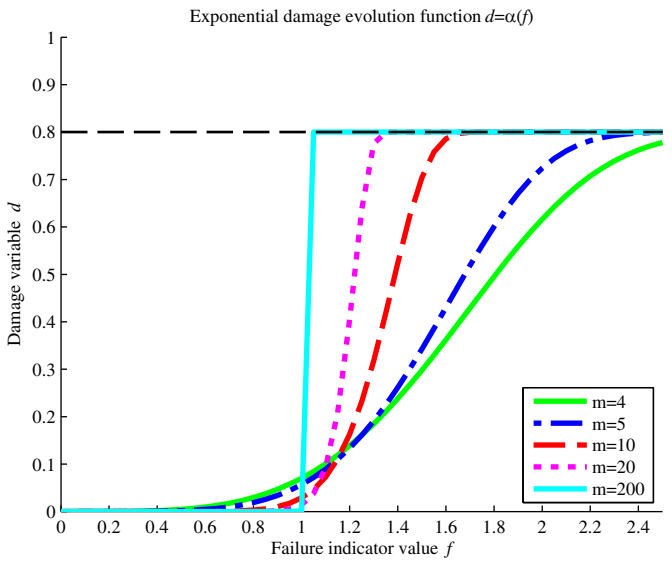

Fig. 5. Damage variable value d as a function of the failure indicator f using the exponential damage evolution function $\alpha(f)$ with $d_{max} = 0.80$ evaluated at various values of the material response parameter m.

$$d_{2max} = \begin{cases} 0.86, & \text{if tension} \\ 0.60, & \text{if compression} \end{cases} \quad (5)$$

Shear damage, listed in Table 8, was considered to be a combination of longitudinal and transverse damage, and was therefore dependent upon the material degradation factors for each. With failure criteria, damage variable definitions, damage evolution laws and material degradation factors determined, the progressive damage model was complete. Similar formulations can be found in Refs. [19,22,41–44].

5. Model validation, results and discussion

Focus was placed on damage onset and initial propagation for both the numerical model and previous experimental work. Model-predicted and experimentally observed failure modes and the bearing stress-strain response were compared to evaluate the performance of the model. The following section discusses the degree of correlation.

At low bearing strain, as also described in ASTM D5961 [35], the bearing stress-strain response may show variation due to joint friction, hole tolerance, joint translation and straightening to overcome small eccentricities in the experimental setup. For this reason, a strain correction is placed on experimental data. The bearing chord stiffness is calculated and, using that calculated stiffness, the linear-elastic region is extrapolated back to zero stress. The data is then shifted so that a linear stress-strain response is seen beginning at zero stress and zero strain. All of the comparisons presented show the experimental data with extrapolation.

A combination of multiple failure modes were determined experimentally for composites reinforced with a three-dimensional woven ply to ply preform when subjected to single-bolt, double-shear bearing. These failure modes, described in detail in Ref. [5], include longitudinal compressive failure of warp tows, transverse weft tow bunching and compressive failure and matrix cracking. At low to moderate bearing strains, these failure modes combined to create bearing-type failures. As bearing strain became increasingly higher, significant transverse weft tow bunching and compressive failure resulted in thickness increases near the hole. The additive effect of this material degradation at high bearing strain led to late shear cracking and shear-out failures. In general, model-predicted damage in both the matrix and warp and weft tows matches that of traditional bearing stresses seen in an isotropic material. For the geometric locations referred to in the following damage discussion, refer to Fig. 3.

Matrix and tow damage were considered separately in the model. Tow damage was separated into warp and weft longitudinal, transverse and combined shear, representing the damage variables used to affect damage on the elastic tow properties. Warp and weft tow damage in the bearing area is seen at various levels of bearing strain in Fig. 6 and Fig. 7, respectively. Longitudinal (1-direction) tensile and compressive stress locations are indicated in Fig. 8 for both the warp and weft tows at 2.2% bearing strain. On either side of the hole towards the edge of the sample, tensile stresses develop along the net section. At the same time, compressive stresses are found along the bearing surface itself, with shear stress propagating from the hole towards the free surface. At the onset of damage, warp tows are found in the model to experience tensile stresses on both edges of the hole and compressive stresses along the middle of the bearing surface. Weft tows experience transverse tension on the sides of the hole and transverse compression along the middle of the bearing surface. Longitudinal weft tows experience tension as bearing failure and weft tow bunching developed.

Matrix damage, as described previously, was calculated using instantaneous damage and a maximum principal stress criterion. Fig. 9 shows matrix damage at different levels of strain in the bearing area. The predicted damage within the matrix material corresponds to what one might expect from an isotropic material bearing response. Predicted by the model, tensile damage first develops on either side of the hole in the matrix material with compressive matrix damage along the bearing surface. Joining the two regions around the circumference of the hole is damage caused by matrix shear. Overall, model-predicted damage and failure modes have good agreement with previous experimental results [5].

Discussed earlier was the applicability of implicit finite element modeling in the case of a zero-stiffness bearing response. Marking the end of its ability to continue capturing the material response, the implicit model developed in this paper was terminated at the end of the transition zone between the linear-elastic and zero-stiffness responses. The end of this transition zone corresponds to a damaged state where the entire weft tow column directly along the bearing surface is predicted to have been completely damaged. The bearing stress-strain responses found experimentally [5] and with the progressive damage model with exponential damage

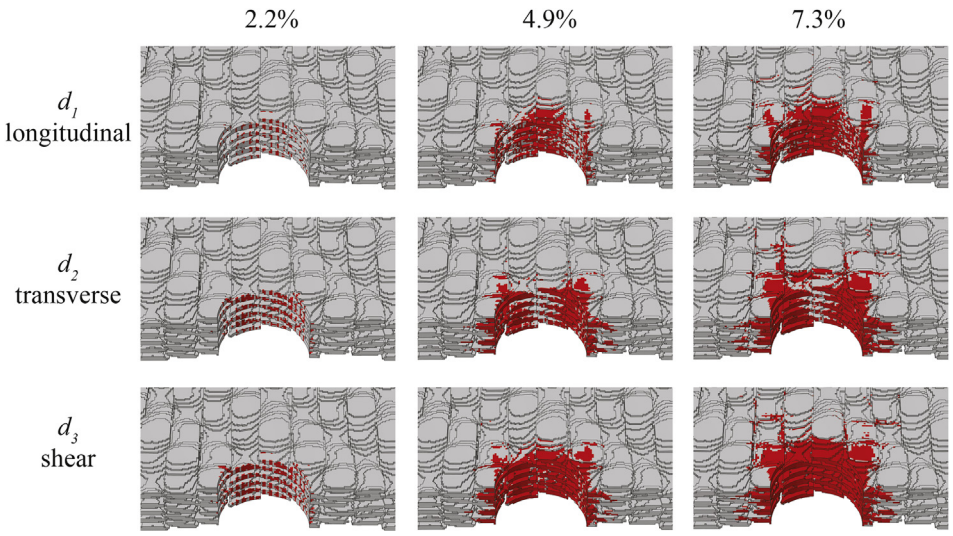

Fig. 6. Warp tow damage propagation at various levels of bearing strain.

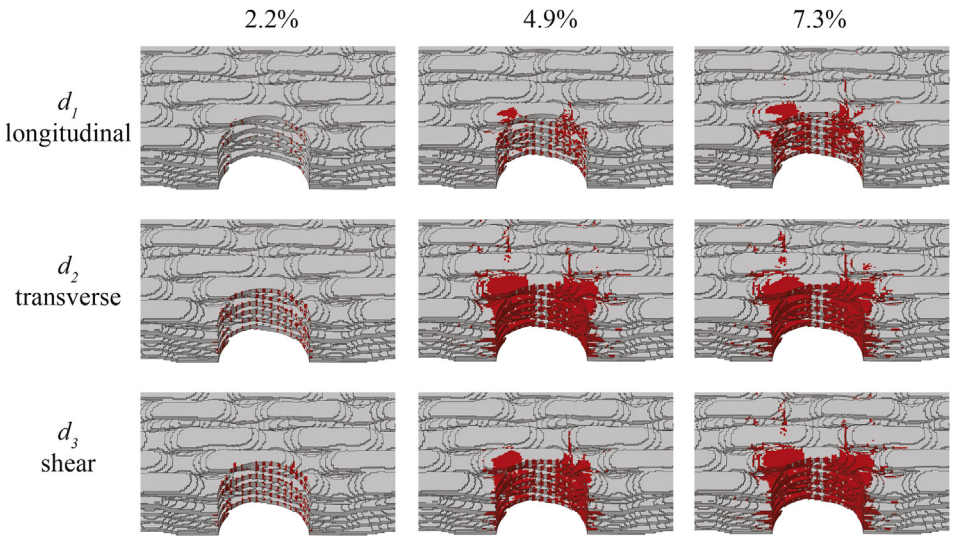

Fig. 7. Weft tow damage propagation at various levels of bearing strain.

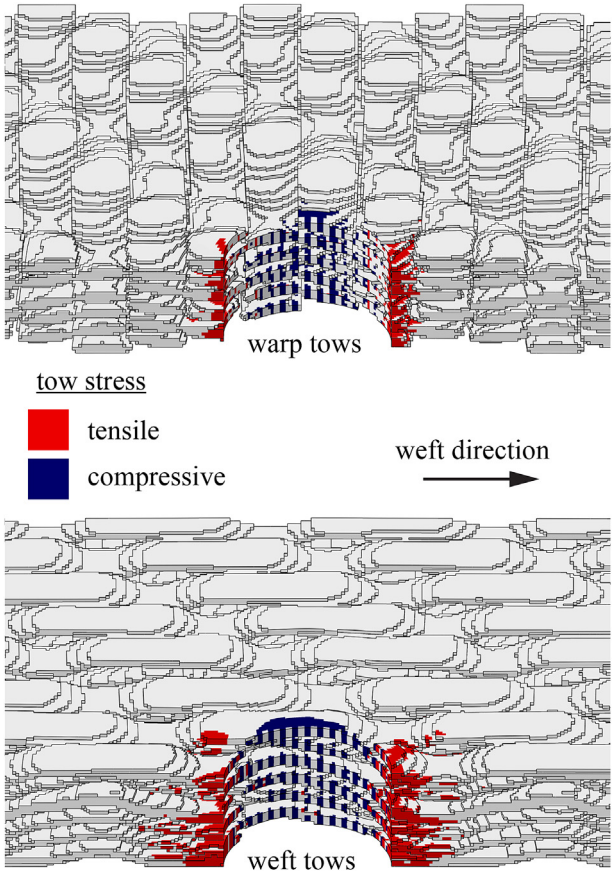

Fig. 8. Longitudinal (1-direction) warp tow (top) and weft tow (bottom) tensile and compressive stress development at 2.2% bearing strain.

evolution and a material response parameter $m = 5$ are seen in Fig. 10. The correlation between the two shows that the progressive damage model not only captures failure modes, but also captures a similar stress-strain response. At 7.3% bearing strain, the model-predicted bearing stress was 3.7% higher than the experimentally measured bearing stress.

To complement the experimental findings from previous work, micro computed tomography imaging was used to explore the onset of bearing damage. Taken from an experimental sample subjected to 9% bearing strain prior to unloading, Fig. 11 further illustrates failure modes that contribute to bearing failure. This sample was evaluated in a single-bolt, double-shear configuration. The fixture used during experimentation generated a thickness-constrained region in the sample around the hole. This constraint has a tendency to shift bearing damage to just outside of this region, which is also depicted in Fig. 11 and explained in more detail in Ref. [5]. The cross-sectional view noted in Fig. 11 is described in Fig. 12 which illustrates the through-thickness damage seen in weft tows. Agreement is seen between the failure modes predicted by the progressive damage model, the micro computed tomography imaging, and experimental observations.

A sensitivity study was conducted involving the damage evolution parameter m and the time step between increments in the finite element model. As the exponential damage evolution parameter m increases, the level of damage in the affected elements is prescribed at a faster rate; the larger the value of m, the more brittle the material failure becomes. Fig. 13 illustrates how various values for the damage evolution parameter can affect a typical bearing stress-strain response. As discussed previously, this progressive damage model is also dependent upon the time step. The smaller the time step, the more accurate the model-predicted behavior will be when compared to the actual material response. Fig. 14 shows various time steps used to complete the prescribed fastener displacement. 25 increments were found to be sufficiently small enough to result in a converged solution while providing an efficient model run time. An exponential damage evolution parameter of 5.0 combined with 25 increments in the progressive damage model produce a material response that predicts damage onset and failure modes seen in experimental evaluation.

6. Conclusions

A progressive damage model has been developed to predict the material response for a composite material reinforced with a three-dimensional woven ply to ply fiber architecture subjected to single-bolt, double-shear bearing. The model incorporates Hashin failure criteria to calculate the value of multiple damage variables used during analysis. Model-predicted failure modes and damage

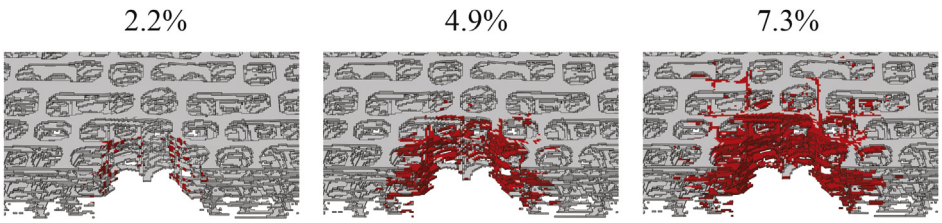

Fig. 9. Matrix damage at various levels of bearing strain.

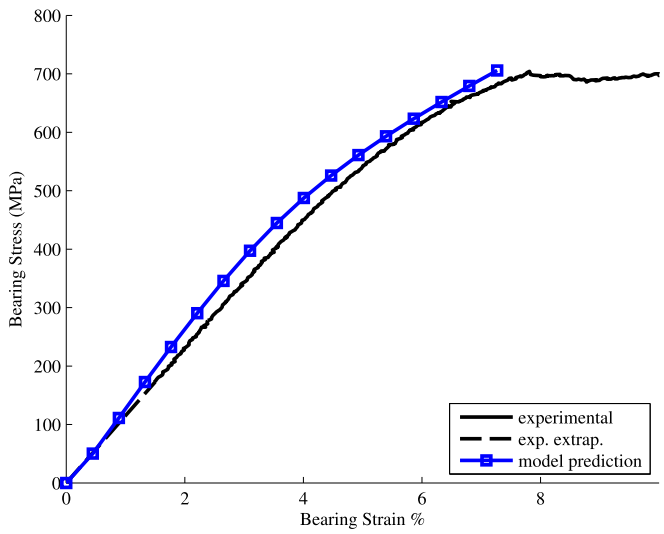

Fig. 10. Model-predicted bearing stress-strain response with exponential damage evolution and material response parameter $m = 5$ compared with typical experimental results [5].

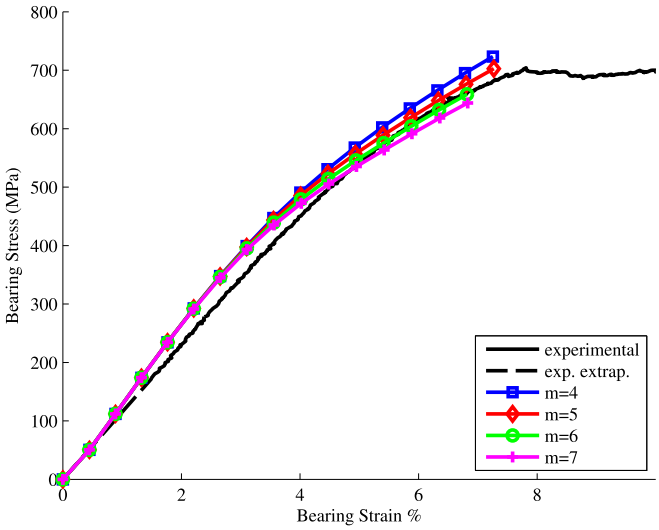

Fig. 13. Damage evolution parameter sensitivity on stress-strain response compared with typical experimental results.

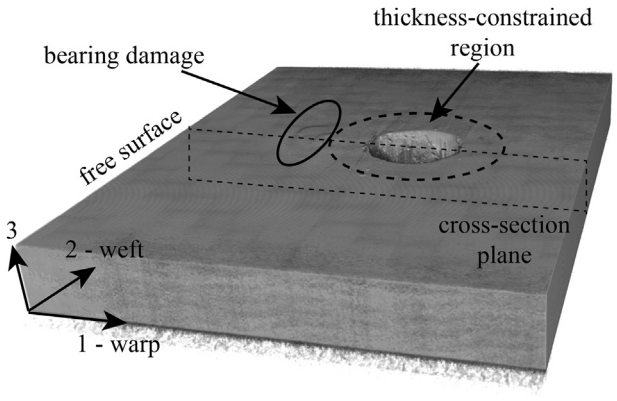

Fig. 11. Bearing damage from micro computed tomography imaging.

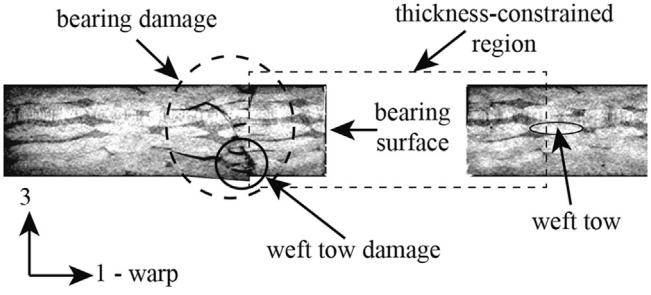

Fig. 12. Micro computed tomography cross-section.

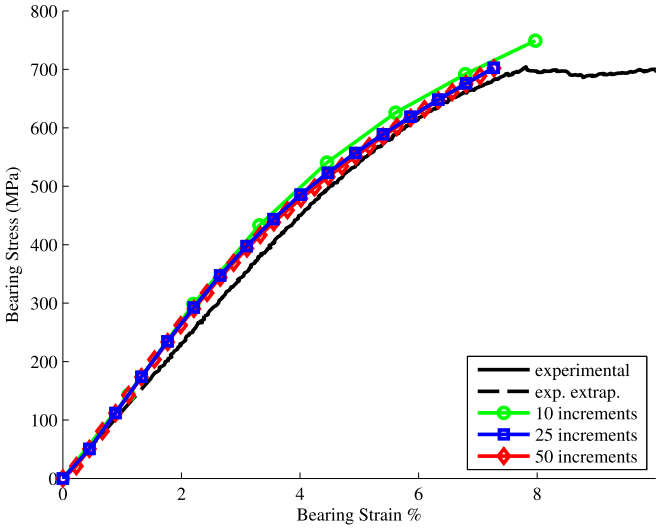

Fig. 14. Implicit model fixed time step size sensitivity on stress-strain response compared with typical experimental results.

correlate well with experimental observations and trends. While this progressive damage model was implemented in a single-bolt, double-shear bolted joint configuration, the same model could be extended to a multi-fastener joint. Additionally, with a mesoscale model with matrix and impregnated tow phases, the geometry of the fiber reinforcement could be changed without modification to the progressive damage model to include different tow sizes, alternative three-dimensional woven architectures or more

traditional two-dimensional woven composites. Significant conclusions from this paper include:

1. A non-linear three-dimensional progressive damage model was developed and applied to the unique as-molded morphology of three-dimensional woven composites using Hashin failure criteria and the MLT damage model.
2. The implemented implicit finite element model can be used to predict the onset and initial propagation of damage in three-dimensional woven composite joints, which is relevant for joint design and expanded industrial application.
3. Material behavior predicted in the progressive damage model, including trends seen in the stress-strain response and failure modes, were validated by experimental findings with good correlation.

Acknowledgments

This research was supported by Albany Engineered Composites. The first author was supported in part by the Sakellaris Graduate Fellowship through the College of Engineering at the University of Maine.

References

[1] Bogdanovich AE. Multi-scale modeling, stress and failure analyses of 3-D woven composites. J Mater Sci 2006;41(20):6547–90. ISSN 0022-2461.
[2] Brandt J, Drechsler K. Manufacture and performance of carbon/epoxy 3-D woven composites. In: 37th International SAMPE Symposium; 1992. p. 864–77.
[3] McClain M, Goering J. Overview of recent developments in 3D structures. In: SME Composites Manufacturing; 2012. p. 1–12.
[4] Warren K, Lopez-Anido R, Goering J. Experimental investigation of three-dimensional woven composites. Compos Part A Appl Sci Manuf 2015a;73:242–59.
[5] Warren K, Lopez-Anido R, Goering J. Behavior of three-dimensional woven carbon composites in single-bolt bearing. Compos Struct 2015b;127:175–84. http://dx.doi.org/10.1016/j.compstruct.2015.03.022.
[6] Warren K, Lopez-Anido RA, Redman C, McClain M. Experimental investigation of single-bolt, single-shear joints in three dimensional woven carbon composites. In: SAMPE 2014; 2014. p. 12.
[7] McCarthy M, McCarthy C. Finite element analysis of effects of clearance on single shear composite bolted joints. Plast Rubber Compos 2003;32(2):65–70. ISSN 1465-8011.
[8] Perugini P, Riccio A, Scaramuzzino F. Three-dimensional progressive damage analysis of composite joints. In: 8th International Conference on Civil and Structural Engineering Computing, Paper; 2001.
[9] Riccio A, Scaramuzzino F. Influence of damage onset and propagation on the tensile structural behavior of protruding composite joints. In: 4th GRACM Congress on Computation Mechanics GRACM; 2002. p. 27–9.
[10] McCarthy M, Lawlor V, Stanley W, McCarthy C. Bolt-hole clearance effects and strength criteria in single-bolt, single-lap, composite bolted joints. Compos Sci Technol 2002;62(10):1415–31. ISSN 0266-3538.
[11] Stanley W, McCarthy M, Lawlor V. Measurement of load distribution in multi-bolt, composite joints, in the presence of varying clearance. J Plast Rubber Compos 2002;31(9):412–8.
[12] McCarthy M, Lawlor V, Stanley W. An experimental study of bolt-hole clearance effects in single-lap, multibolt composite joints. J Compos Mater 2005a;39(9):799–825. ISSN 0021-9983.
[13] Ireman T. Three-dimensional stress analysis of bolted single-lap composite joints. Compos Struct 1998;43(3):195–216. ISSN 0263-8223.
[14] McCarthy M, McCarthy C, Lawlor V, Stanley W. Three-dimensional finite element analysis of single-bolt, single-lap composite bolted joints: part I - model development and validation. Compos Struct 2005b;71(2):140–58. ISSN 0263-8223.
[15] McCarthy C, McCarthy M. Three-dimensional finite element analysis of single-bolt, single-lap composite bolted joints: part II - effects of bolt-hole clearance. Compos Struct 2005;71(2):159–75. ISSN 0263-8223.
[16] Hashin Z. Failure criteria for unidirectional fiber composites. J Appl Mech 1980;47(2):329–34. ISSN 0021-8936.
[17] Camanho P, Matthews F. A progressive damage model for mechanically fastened joints in composite laminates. J Compos Mater 1999;33(24):2248–80. ISSN 0021-9983.
[18] Wang H-S, Hung C-L, Chang F-K. Bearing failure of bolted composite joints. Part I: experimental characterization. J Compos Mater 1996;30(12):1284–313. ISSN 0021-9983.
[19] Tan SC. A progressive failure model for composite laminates containing openings. J Compos Mater 1991;25(5):556–77. ISSN 0021-9983.
[20] Nuismer R, Tan S. Constitutive relations of a cracked composite lamina. J Compos Mater 1988;22(4):306–21. ISSN 0021-9983.
[21] Tan S, Nuismer R. A theory for progressive matrix cracking in composite laminates. J Compos Mater 1989;23(10):1029–47. ISSN 0021-9983.
[22] Tan SC, Perez J. Progressive failure of laminated composites with a hole under compressive loading. J Reinf Plast Compos 1993;12(10):1043–57. ISSN 0731-6844.
[23] Xiao Y, Ishikawa T. Bearing strength and failure behavior of bolted composite joints (part I: experimental investigation). Compos Sci Technol 2005a;65(7):1022–31. ISSN 0266-3538.
[24] Xiao Y, Ishikawa T. Bearing strength and failure behavior of bolted composite joints (part II: modeling and simulation). Compos Sci Technol 2005b;65(7):1032–43. ISSN 0266-3538.
[25] Zhou Y, Lu Z, Yang Z. Progressive damage analysis and strength prediction of 2D plain weave composites. Compos Part B Eng 2013;47:220–9. ISSN 1359-8368.
[26] Lomov SV, Ivanov DS, Verpoest I, Zako M, Kurashiki T, Nakai H, et al. Meso-FE modelling of textile composites: road map, data flow and algorithms. Compos Sci Technol 2007;67(9):1870–91. ISSN 0266-3538.
[27] Lomov SV, Ivanov DS, Verpoest I, Zako M, Kurashiki T, Nakai H, et al. Full-field strain measurements for validation of meso-FE analysis of textile composites. Compos Part A Appl Sci Manuf 2008;39(8):1218–31. ISSN 1359-835X.
[28] Lomov SV, Bogdanovich A, Ivanov D, Hamada K, Kurashiki T, Zako M. Finite element modelling of progressive damage in non-crimp 3D orthogonal weave and plain weave E-glass composites. In: Proceedings of the 2nd world conference on 3D fabrics; 2009.
[29] Tsukrov I, Bayraktar H, Giovinazzo M, Goering J, Gross T, Fruscello M, et al. Finite element modeling to predict cure-induced microcracking in three-dimensional woven composites. Int J Fract 2011;172(2):209–16. ISSN 0376-9429.
[30] Ansar M, Xinwei W, Chouwei Z. Modeling strategies of 3D woven composites: a review. Compos Struct 2011;93(8):1947–63. ISSN 0263-8223.
[31] ASTM Standard D3039. Standard test method for tensile properties of polymer matrix composite materials. West Conshohocken, PA: ASTM International; 2008.
[32] ASTM Standard D6641. Standard test method for compressive properties of polymer matrix composite materials using a combined loading compression (CLC) test fixture. West Conshohocken, PA: ASTM International; 2009.
[33] ASTM Standard D7078. Standard test method for shear properties of composite materials by V-notched rail shear method. West Conshohocken, PA: ASTM International; 2005.
[34] CYCOM PR 520 RTM Resin System. Cytec engineered materials. 2012.
[35] ASTM Standard D5961. Standard test method for bearing response of polymer matrix composite laminates. West Conshohocken, PA: ASTM International; 2010.
[36] Drach A, Brach B, Tsukrov I, Bayraktar H, Goering J. Realistic FEA modeling of 3D woven composites on mesoscale. In: International Conference on Composite Materials; 2013. p. 1813–20.
[37] Matzenmiller A, Lubliner J, Taylor R. A constitutive model for anisotropic damage in fiber-composites. Mech Mater 1995;20(2):125–52. ISSN 0167-6636.
[38] Kermanidis T, Labeas G, Tserpes K, Pantelakis S. Finite element modeling of damage accumulation in bolted composite joints under incremental tensile loading. In: Proceedings of the Third ECCOMAS Congress; 2000. p. 11–4.
[39] Hung C-L, Chang F-K. Bearing failure of bolted composite joints. Part II: model and verification. J Compos Mater 1996;30(12):1359–400. ISSN 0021-9983.
[40] McCarthy C, McCarthy M, Lawlor V. Progressive damage analysis of multi-bolt composite joints with variable bolt-hole clearances. Compos Part B Eng 2005c;36(4):290–305. ISSN 1359-8368.
[41] Chang F-K, Chang K-Y. A progressive damage model for laminated composites containing stress concentrations. J Compos Mater 1987;21(9):834–55. ISSN 0021-9983.
[42] Maa R-H, Cheng J-H. A CDM-based failure model for predicting strength of notched composite laminates. Compos Part B Eng 2002;33(6):479–89. ISSN 1359-8368.
[43] Li H-S, Xia S, Luo D-M. A probabilistic analysis for pin joint bearing strength in composite laminates using subset simulation. Compos Part B Eng 2014;56:780–9. ISSN 1359-8368.
[44] Wang X, Zhang J, Wang Z, Liang W, Zhou L. Finite element simulation of the failure process of single fiber composites considering interface properties. Compos Part B Eng 2013;45(1):573–80. ISSN 1359-8368.